Comparative analysis of crystal-field parameters for rare-earth ions at monoclinic sites in $AB(WO_4)_2$ crystals: I. Tm^{3+} in $KGd(WO_4)_2$ and $KLu(WO_4)_2$, and Ho^{3+} and Er^{3+} ions in $KGd(WO_4)_2$

2010 J. Phys.: Condens. Matter 22 045501

(http://iopscience.iop.org/0953-8984/22/4/045501)

J. Phys.: Condens. Matter **22** (2010) 045501 (11pp) doi:10.1088/0953-8984/22/4/045501

Comparative analysis of crystal-field parameters for rare-earth ions at monoclinic sites in $AB(WO_4)_2$ crystals: I. Tm^{3+} in $KGd(WO_4)_2$ and $KLu(WO_4)_2$, and Ho^{3+} and Er^{3+} ions in $KGd(WO_4)_2$

Czesław Rudowicz and Paweł Gnutek

Institute of Physics, West Pomeranian University of Technology, Aleja Piastów 17, 70-310 Szczecin, Poland

E-mail: crudowicz@zut.edu.pl

Received 5 November 2009, in final form 3 December 2009
Published 5 January 2010
Online at stacks.iop.org/JPhysCM/22/045501

Abstract

The crystal-field (CF) parameters determined by various authors for rare-earth ions at monoclinic sites in $AB(WO_4)_2$ crystals are reanalyzed using a methodology incorporating several approaches, namely standardization, multiple-correlated fitting technique and closeness of CFP sets. In Part I recent spectroscopic data for Tm^{3+} ions in $KGd(WO_4)_2$ (KGdW) and $KLu(WO_4)_2$ (KLuW), and Ho^{3+} and Er^{3+} ions in KGdW, which were interpreted using the free-ion (FI) and CF parameter (CFP) sets, are thoroughly revisited. Our reanalysis enables clarification of several doubtful aspects involved in the previous studies. The initial CFPs for fitting, calculated using the simple overlap model (SOM), differ markedly from the fitted CFPs for Tm^{3+} ions in KGdW and KLuW. An inspection of the pertinent CFP sets reveals deeper *intrinsic* differences between the model and fitted CFPs. The model CFPs and the fitted CFPs for RE^{3+} ions in both KGdW and KLuW crystals turn out to be non-standard. Importantly, the model and fitted CFP sets for Tm-KLuW belong to disparate regions of the CFP space and thus are *intrinsically incompatible*, i.e. such sets should not be directly compared. Thus the CFP sets reported in the literature require reconsideration in view of the intrinsic properties of monoclinic CF Hamiltonians previously not taken into account. Standardization of the originally non-standard CFP sets is carried out to ensure direct comparability of the CFP sets in question with other literature data. The correlated alternative CFP sets are calculated for each original set to facilitate future applications of the multiple correlated fitting technique, which enables improving overall reliability of the fitted CFPs. The closeness of the standardized CFP sets is assessed in a quantitative way. Our considerations indicate also the importance of proper definitions of the axis system used in the CFP model calculations and provide arguments for the *nominal* meaning of the axis systems assigned to the fitted CFPs. The consistent methodology proposed here may be considered as a general framework for analysis of CF levels and CFP modelling for rare-earth and transition-metal ions at monoclinic symmetry sites in crystals. CFP sets for other rare-earth ions in $AB(WO_4)_2$ crystals will be reanalyzed in Part II.

1. Introduction

Accurate modelling of crystal-field (CF) interactions and interpretation of optical absorption spectra is important for a proper understanding of the characteristics important for potential applications of luminescent and laser materials as well as extracting useful information on the spectroscopic properties of the $4f^N$ rare-earth (RE) and $3d^N$ transition-metal ions doped into host crystals [1–8]. An important class of materials with applications in optoelectronics as solid state lasers consists of crystals with the formula $AB(WO_4)_2$ doped with RE^{3+} ions. For this purpose, spectroscopic characterization has recently been carried out for, for example, Tm^{3+} [9, 10] and Er^{3+} [11] ions in $KGd(WO_4)_2$ (KGdW), Tm^{3+} ions in $KLa(WO_4)_2$ [12] and Dy^{3+} ions in $KY(WO_4)_2$ [13]. Subsequently, CF analysis and fitting of the crystal-field parameters (CFPs) followed. This is an increasingly difficult task with the lowering of the site symmetry of RE^{3+} ions [4, 5]. Yet the intrinsic properties of the orthorhombic [14, 15], monoclinic [16–18] and triclinic [19, 20] CF Hamiltonians, which bear significantly on the meaningfulness of CF studies, appear to be not fully recognized by some authors, as discussed in the review [21]. Recent examples of an apparent unawareness of these properties are provided by optical spectroscopy studies of laser crystals doped with RE^{3+} ions: Tm^{3+} ions in KGdW and $KLu(WO_4)_2$ (KLuW) [22], and Ho^{3+} and Er^{3+} ions in KGdW [23].

In this paper we present a consistent methodology for CF analysis for transition ions at monoclinic (C_s, C_2, C_{2h}) sites in crystals taking into account the intrinsic properties of monoclinic CF Hamiltonians [16–20]. Using this methodology recent Pujol's *et al* CFP sets for Tm^{3+} ions in KGdW and KLuW [22], and Ho^{3+} and Er^{3+} ions in KGdW [23], are reanalyzed in Part I, whereas CFP sets for Pr^{3+} and Nd^{3+} ions in other $AB(WO_4)_2$ crystals [24–26] will be dealt with in Part II. Optical absorption measurements [22] were interpreted using ten free-ion parameters and 15 monoclinic CFPs expressed in the Wybourne notation [1, 4, 5]. In total over 50 experimental CF energy levels arising from the Tm^{3+} ($4f^{12}$) electronic configuration were identified in the optical spectra and assigned for each crystal. To obtain reliable starting CFPs, the simple overlap model (SOM) calculations [27, 28] were carried out in the initial phase of CF analysis [22]. Simultaneous fittings of the 24 parameters, with some constraints on the free-ion parameters and the 'imaginary' part of the second-rank CFP Im B_{22} set to zero (i.e. the R approach defined in [16, 18]), yielded the fitted CFPs differing markedly from the SOM-determined CFPs for Tm^{3+} ions in both KGdW and KLuW.

An inspection of the CFP sets [22, 23] reveals, however, that the model CFPs and the fitted CFPs [22] for RE^{3+} ions in both crystals are non-standard [14, 16]. Importantly, the model and fitted CFP sets for Tm-KLuW [22] belong to disparate regions of the CF parameter space. Such CFP sets are *intrinsically incompatible* [21] and, in spite of their *apparent* general closeness, should not be directly compared [17, 18, 21]. The authors [22, 23] seem to be unaware of the intrinsic properties of the orthorhombic [14, 15] and monoclinic [16–20] CF Hamiltonians, recently reviewed in [21]. The present paper addresses the problems involved in the CF studies of Tm^{3+} ions in KGdW and KLuW [22] as well as Ho^{3+} and Er^{3+} ions in KGdW [23], which bear profoundly on reliability of theoretical and experimental CFPs. The available CFP sets are reanalyzed using methodology incorporating several approaches worked out by us earlier, namely, standardization, multiple correlated fitting technique and closeness of CFP sets [14–20]. Our considerations enable clarification of several doubtful aspects involved in the studies [22, 23] as well as an explanation of the apparent disparity between the model CFP sets and the fitted CFP sets for Tm^{3+} ions in KGdW and KLuW determined by Pujol *et al* [22].

This paper is organized as follows. In section 2 theoretical background and methodology for the analysis of monoclinic CFP sets is briefly outlined. General aspects requiring clarification in Pujol's *et al* [22, 23] studies are considered in section 3. Comparative analysis of CFPs for Tm^{3+} ions in KGdW and KLuW, and Ho^{3+} and Er^{3+} ions in KGdW, is carried out in section 4. Finally, a summary and conclusions are provided in section 5.

2. Theoretical background and methodology for analysis of monoclinic CFP sets

The total Hamiltonian for the energy level calculations and fitting the observed energy levels for $4f^N$ ions in crystals consists of the free-ion ($H_{\rm FI}$) terms, which is spherically symmetric and need not to be considered here, and crystal-field ($H_{\rm CF}$) terms, which depend on the local site symmetry. In the compact form [29] $H_{\rm CF}$ is expressed in the Wybourne notation as [1, 4, 5]

$$H_{\rm CF} = \sum_{k,q} B_{kq} C_{kq}(x, y, z) \tag{1}$$

with $k = 2$, 4 and 6. The number of non-vanishing CFP components q in equation (1) depends on the local site symmetry [1–8]. For a review of the operator and parameter notations used in optical spectroscopy and the EMR area, see [29, 30].

For monoclinic symmetry the axis system (x, y, z) in equation (1) may be chosen with respect to the monoclinic symmetry C_2 axis (or monoclinic direction) in one of three different ways, i.e. $C_2 \| z$, $C_2 \| x$ or $C_2 \| y$ [16–18]. The case $C_2 \| x$ and $C_2 \| y$ corresponds to the transformation of the axis system ($xyz \rightarrow yzx$) and ($xyz \rightarrow zxy$), respectively. Each of these three physically equivalent cases corresponds to a specific form of the CF Hamiltonian and thus yields a different set of CFPs. The case $C_2 \| z$ is most frequently employed in the literature and corresponds to $H_{\rm CF}$:

$$\begin{aligned} H_{\rm CF} = {} & B_{20}C_{20} + \mathrm{Re}\, B_{22}(C_{22} + C_{2-2}) + \mathrm{Im}\, B_{22}(C_{22} - C_{2-2}) \\ & + B_{40}C_{40} + \mathrm{Re}\, B_{42}(C_{42} + C_{4-2}) + \mathrm{Im}\, B_{42}(C_{42} - C_{4-2}) \\ & + \mathrm{Re}\, B_{44}(C_{44} + C_{4-4}) + \mathrm{Im}\, B_{44}(C_{44} - C_{4-4}) \\ & + B_{60}C_{60} + \mathrm{Re}\, B_{62}(C_{62} + C_{6-2}) \\ & + \mathrm{Im}\, B_{62}(C_{62} - C_{6-2}) + \mathrm{Re}\, B_{64}(C_{64} + C_{6-4}) \end{aligned}$$

$$+ \operatorname{Im} B_{64}(C_{64}{-}C_{6-4}) + \operatorname{Re} B_{66}(C_{66} + C_{6-6}) + \operatorname{Im} B_{66}(C_{66}{-}C_{6-6}). \quad (2)$$

For the intrinsic properties of the orthorhombic [14, 15], monoclinic [16, 17] and triclinic [18–20] CF Hamiltonians the readers may consult the pertinent references. The reanalysis of the papers [22, 23] in sections 3 and 4 indicates that the authors have apparently been unaware of the intrinsic properties in question.

Due to the general properties of the symbolic CFPs [18] in equation (2), the parameter $\operatorname{Im} B_{22}$ in equation (2) may be set to zero by a suitable rotation by the angle α about the z axis, denoted 'α/Oz', determined by the ratio of the original CFPs [16]:

$$\tan(2\alpha) = \operatorname{Im} B_{22}/\operatorname{Re} B_{22}. \quad (3)$$

Thus, the number of parameters in H_{CF} in equation (2) may be reduced by one. Note that reduction of the transformed (primed) $\operatorname{Im} B'_{22} = 0$ yields the CFP sets expressed in the principal axis system of the second-rank CF terms [16, 19]. The fitting procedures based on this reduction are classified as the R(reduced) approach, to distinguish from the C(complete) approach employing all monoclinic CFPs in equation (2) or its equivalent forms [16–18]. The R approach has been utilized for the CFP fittings in [22, 23], which is acceptable (see, e.g., [17, 18]). However, as discussed in section 3, the usage of the R approach in the theoretical SOM calculations in [22] is inappropriate.

The standardization of CF Hamiltonians [14–20] is utilized to ensure direct comparability of the CFP sets taken from various sources [21]. The orthorhombic standardization is based on limiting the rhombicity ratio:

$$\kappa = \operatorname{Re} B_{22}/B_{20} \quad (4)$$

in the Wybourne notation [1, 4, 5] to the standard range $(0,\ 1/\sqrt{6} \approx 0.408)$ and is equivalent to the condition of the maximal values of B_{k0} axial parameters [31]. Choices for assigning the orthorhombic symmetry axes are provided in appendix A. The orthorhombic standardization idea [14] has been extended and applied to monoclinic [16–18] and triclinic H_{CF} [19, 20]. Importantly, for the lower symmetry cases CFP sets must be first expressed in the principal axis system of the second-rank CF terms [16–21]. A review of specific applications of standardization for analysis of orthorhombic and lower symmetry CFP sets has been provided in [21]. The standardization transformations $S2$–$S6$ [14] (see appendix A) are performed on the original sets $S1$ using the CST package [32]. The 'pure' orthorhombic and 'pure' monoclinic terms in H_{CF}, equation (2), transform under the standardization transformations Si independently from each other, e.g. $\operatorname{Im} B_{22}$ becomes $\operatorname{Im} B_{21}$ or $\operatorname{Re} B_{21}$ [16]. Orthorhombic and monoclinic standardization transformations of CFPs in the Wybourne notation are listed explicitly in appendix B.

The intricate low symmetry aspects inherent in the spectroscopic studies [22, 23] and the resulting monoclinic CFP sets are reanalyzed in sections 3 and 4, respectively. Our methodology incorporates the following approaches: standardization of CF Hamiltonians [14, 16], multiple correlated fitting technique [16] and closeness of CFP sets [15, 18, 33, 34]. Our considerations enable clarification of several doubtful aspects identified in [22, 23]. The concept of standardization of CF Hamiltonians [14, 16] is utilized to ensure direct comparability of the CFP sets under consideration [21]. Standardization of CFP sets calls for corrections to the CFP systematics across the RE series presented in [22, 23]. Various alternative CFP sets are calculated for possible applications of the multiple correlated fitting technique [16], which would enable improving overall reliability of the fitted CFPs [17, 18]. Closeness of standardized CFP sets is quantitatively assessed using the closeness factors and the norm ratios [15, 18, 33, 34].

3. General aspects requiring clarification

Critical examination of the papers [22, 23] reveals several doubtful aspects that may be categorized as discussed below. Points (ii)–(v) below indicate convincingly the importance of proper definitions of the axis system used in model calculations of CFPs as well as provide arguments for the *nominal* meaning of the axis systems that can be assigned to the fitted CFP sets.

(i) Notation for CFP symbols

Due to the Hermitian properties of the operators C_{kq} in equation (1) the relation: $B_{k-q} = (-1)^q B_{kq}$ holds and thus B_{kq} may be represented as $B_{kq} = \operatorname{Re} B_{kq} + \mathrm{i} \operatorname{Im} B_{kq}$, see, e.g., [1, 4, 35, 20]. In fact, the symbols B^k_q for the real parts of CFPs and $\mathrm{i}B^k_q$ for the imaginary ones were used in [22], instead of the proper ones $\operatorname{Re} B_{kq}$ and $\operatorname{Im} B_{kq}$ [1, 4, 35, 20], respectively. The notation $\mathrm{i}B^k_q$ is misleading as it represents a multiplication of a given parameter by $\mathrm{i} = \sqrt{-1}$. Moreover, the symbols B^k_q and $\mathrm{i}B^k_q$ used in [22] and those B^k_q and $\mathrm{i}S^k_q$ used in [23] confusingly resemble the extended Stevens operator notation [36, 29]. It appears that this notation may have been taken over from Porcher *et al* [27]. Note that Pujol *et al* [22] use the inverted sequence of operators in the monoclinic terms, namely $\mathrm{i}B^k_q(C^k_{-q} - C^k_q)$, whereas in the earlier paper [23] the sequence: $\mathrm{i}S^k_q(C^k_q - (-1)^q C^k_{-q})$ was used. Hence, the signs of all CFPs $i\,B^k_q$ in [22], i.e. $\operatorname{Im} B_{kq}$, should be formally inverted as compared with the notation in [23], which prevails in the literature: $\operatorname{Im} B_{kq}(C_{kq} - C_{k-q})$ [1–5]. However, judging by the correspondence of signs in [22] and [23], we assume that the CF Hamiltonian in equation (3) in [22] is rather incorrectly presented, whereas the CFPs in table 4 of [22] conform to the usual sign conventions.

(ii) Distinction between the meaning of the symbolic, model, and fitted CFPs

There is an evident lack of distinction between the meaning of the symbolic, model, and fitted CFPs. The properties of the distinct types of CFPs have been overlooked in [22] thus leading partially to the consequences discussed in section 4. The CFPs in equations (1) and (2) have only a symbolic meaning as defined in [18]. It should be kept in mind that the

form of H_{CF} depends on the axis system and the simplest form is obtained in the symmetry-adapted axis system [18]. The two other types of CFPs involved in optical studies, namely the model CFPs and the fitted CFPs, have distinct properties from those of the symbolic CFPs used in a specific H_{CF} form. The model CFPs may be obtained from various theoretical model calculations. As reviewed succinctly in [27], this may include the superposition model (SPM) [37], angular overlap model (AOM) [38, 39] and the exchange charge model (ECM) [40], apart from the SOM [41] used in [22, 23]. Importantly, any model CFP calculations must utilize the crystallographic positions of ligands expressed in a specific axis system. Hence, the model CFP sets must be expressed in that well-defined axis system used to represent the ionic positions of ligands.

In contrast, the fitted CFPs, as discussed in [18], cannot be assigned any particular axis system with known orientation w.r.t. the crystallographic axis system (CAS). The fitted CFPs are obtained by simultaneous diagonalization of the matrix of the Hamiltonian ($H_{FI} + H_{CF}$) within the basis functions $|SLJM_J\rangle$ and fitting the experimental crystal-field levels. Note that the IMAGE f-shell computer package developed by Porcher [42] was used in the CF calculations [22]. In view of the existence of several physically equivalent solutions, each fitted CFP set must be considered as expressed in an undefined axis system, denoted in [18] as a '*nominal*' axis system. The actual orientation in crystal of the '*nominal*' axis system for any fitted CFP set may be determined by comparing the fitted CFP sets, corresponding to given regions of the multiparameter CFP space, with the CFP set obtained from a theoretical model. Hence, only such undefined '*nominal*' axis system, and not the axis system used for the SOM calculations, may be initially assigned to the fitted CFP sets obtained in [22, 23].

(iii) Relative orientation of the axis system used in the SOM calculations w.r.t. the crystallographic axes

Since the Tm-KREW (RE = Gd, Lu) crystals are monoclinic, the crystallographic axis system (CAS): (a, b, c), does not form a Cartesian axis system. Hence, a modified CAS, denoted as CAS*, must be defined with either the a axis or c axis taken as the asterisked axis perpendicular to the b axis and the remaining crystallographic axis. This leaves two options for the modified CAS*: either (a^*, b, c) or (a, b, c^*). The monoclinic C_2 symmetry axis turns out to coincide with the b axis [22]. However, doubts arise concerning the definition of the axis system used in the SOM calculations in [22], since neither the CAS nor CAS* has been explicitly mentioned. An inspection of the SOM [27] listed in [22] has not provided any clue concerning the definition of the axis system actually used in the SOM calculations. Without a clear definition of the axis system, only a tentative comparison of the SOM calculated CFPs [22] with the fitted CFPs and/or other pertinent CFPs obtained by others for related ion–host systems may be made. Additionally, two general comments, namely (iv) and (v) below, are pertinent concerning the orientation of the axis system used in the SOM calculations.

(iv) Appropriateness of the specific monoclinic CF Hamiltonian form employed

Out of three possible physically equivalent forms of monoclinic H_{CF} [16, 18] discussed in section 2, a specific form in equation (2), which corresponds to the case $C_2 \parallel z$, was employed in [22, 23]. However, no proper justification for this choice has been provided by the authors [22, 23]. In order to ensure compatibility of the model and fitted CFPs, this choice should be explicitly adopted in the SOM calculations. However, as discussed in point (iii) above no such consideration has been invoked in [22, 23].

(v) Interpretation and appropriateness of the R approach versus the C approach

The reduction of one CFP by a '*proper choice of the reference axis system, which cancels the complex* iB_2^2', which was used in [22, 23] for the fitted CFPs, is equivalent to the R approach defined in [16]; see also [18, 43]. Importantly, instead of Im B_{22} (iB_2^2) another monoclinic CFP of the higher-rank Im B_{4q} or Im B_{6q} may be set to zero [18, 43]. Note that alternatively any real counterpart CFP Re B_{kq} ($q \neq 0$) may be equally well set to zero. Such choices, so rarely used, represent alternative versions of the R approach [16, 18, 43].

Interpretation of the one-parameter reduction involved in the R approach given in the above quote [22, 23] is commonly presented in the literature. However, in fact, no choice of the reference axis system does take place and such a reduction does not involve any real 'rotation' of the reference axis system. Proper interpretation of the R approach requires taking into account the '*nominal*' meaning of the axis systems assigned to the fitted CFPs [18] discussed in section 3(ii). Hence, any version of the R approach represents a selection, for the fitting procedure, of a particular parametrization for the CFPs out of various parametrization schemes that consist in setting to zero a particular monoclinic symbolic CFP [16, 18, 43]. Importantly, from CF energy levels fittings only the 'length of a vector' $\mathbf{v}_{kq}$ formed by the CFP pairs with a given k: $|\mathbf{v}_{kq}| = (\{\text{Re } B_{kq}\}^2 + \{\text{Im } B_{kq}\}^2)^{1/2}$ may be determined [16, 18].

A more serious misinterpretation of the R approach is its usage in the model calculations in [22]. For monoclinic crystals, the ionic positions of ligands given originally in the non-Cartesian CAS (a, b, c) should be firstly recalculated into the modified CAS*: (a^*, b, c) or (a, b, c^*). Next, with the $b(C_2)$ axis taken as the z axis for the H_{CF} in equation (2), all monoclinic CFPs should be determined from the SOM. Then, the rotation around the z axis by an angle α required to cancel Im B_{22} in equation (3) could be performed to determine the monoclinic angle w.r.t. the modified CAS* used. However, no such procedure has been mentioned in [22]. Even if the SOM CFPs were calculated using a proper Cartesian axis system, since the CFP Im B_{22} was simply omitted from calculations, the model CFP values in table 4 of [22] must be considered as corresponding to the 'unrotated' axis system, in which a non-zero value of Im B_{22} may be expected.

To assess the effect of the incorrect R approach on the SOM-calculated CFP values [22], simulated calculations have been carried out. For illustration, the simulated CFP values for

Table 1. The simulated CFP sets ($C1$–$C5$) for Tm^{3+} ions in KGdW assuming the reasonable values of Im B_{22}, as compared with the values of B_{20} and Re B_{22} in the original set (R) arising from the R approach [22], had the Cx sets been originally obtained from the SOM using the C approach; $S_4 = 474$, $S_6 = 144$ (cm^{-1}).

SOM sets	Original R	$C1$	$C2$	$C3$	$C4$	$C5$
B_{20}	447	447.0	447.0	447.0	447.0	447.0
Re B_{22}	276	293.6	340.9	407.7	486.0	571.1
Im B_{22}	0	$100 \rightarrow 0$	$200 \rightarrow 0$	$300 \rightarrow 0$	$400 \rightarrow 0$	$500 \rightarrow 0$
α	0	−9.958°	−17.964°	−23.693°	−27.697°	−30.551°
κ	0.618	0.657	0.763	0.912	1.087	1.278
B_{40}	−783	−783.0	−783.0	−783.0	−783.0	−783.0
Re B_{42}	269	2.2	−214.0	−359.5	−453.0	−514.4
Im B_{42}	−736	−783.6	−753.8	−696.3	−639.4	−591.2
Re B_{44}	−170	27.7	181.8	260.3	291.3	299.6
Im B_{44}	247	298.6	238.5	148.9	71.3	12.2
B_{60}	−211	−211.0	−211.0	−211.0	−211.0	−211.0
Re B_{62}	205	229.5	229.4	218.3	205.3	193.6
Im B_{62}	108	31.7	−32.8	−77.7	−107.4	−127.3
Re B_{64}	79	76.0	47.4	17.4	−5.6	−21.8
Im B_{64}	24	−32.2	−67.6	−80.7	−82.4	−79.6
Re B_{66}	−168	50.1	199.9	228.4	200.4	158.7
Im B_{66}	156	223.7	112.3	−20.1	−111.4	−165.4
S_2 (cm^{-1})	265	273	294	326	367	413

Tm^{3+} ions in KGdW are provided in table 1. We assume the values of Im B_{22} in a reasonable range as compared with the values of B_{20} and Re B_{22} and then calculate the CFP sets which would have been obtained after reduction of Im B_{22} to zero had the C approach been originally used in the model calculations. As could be expected, inclusion of the non-zero Im B_{22}, which mimics the C approach to be originally used, results after the rotation α/Oz defined in equation (3) in a progressive increase in Re B_{22} with increasing value of Im B_{22}, while by default leaving the parameters B_{k0} invariant. Table 1 indicates convincingly the inappropriateness of using the R approach as the starting point in the SOM calculations. This conclusion is valid also for any other type of model calculations. Since the CFP sets resulting from the mimicking procedure remain non-standard (see table 1), it would be necessary to standardize such sets as discussed in section 2. In principle, the change of the region in the CFP space may be induced for sufficiently large values of Im B_{22}, resulting in CFP sets belonging to the next region corresponding to the greater (absolute) values of the ratio κ (see appendix A). Note that the CFP strength parameters [44, 20] for a given rank S_k ($k = 2, 4, 6$) and the global one S_g used in [22, 23] are invariant under rotations of the axis system. Hence, for all transformed CFP sets the quantities S_k have the same value. However, it is not the case if one CFP is omitted from the SOM calculations as in the R approach used in [22]. This omission yields different values of S_2, whereas the same S_4 and S_6 are obtained for the sets listed in table 1 and denoted $C1$–$C5$.

(vi) General reasons for disparities between CFPs

In many instances it happens that the orthorhombic and lower symmetry standardization provides means to reconcile the differences between CFP sets reported by various authors. Thus this procedure helps to solve the controversial claims about the inaccuracy of the data of fellow researchers [15, 33, 34]. In the case such differences could not be resolved in this way, the reasons for any remaining disparities indicated, e.g. by the observed moderate and not perfect closeness between the standardized CFPs, must be searched for in a different realm. The possible reasons of such disparities may be related either to (i) the factors related to the inherent approximations made in the semi-empirical modelling procedures used, e.g. SOM, AOM, SPM and ECM [27], or (ii) the fitting procedures used to extract the fitted CFP sets from raw experimental data.

In general, other reasons for disparities between CFPs taken from various sources may include, e.g. quality of the experimental energy levels, validity of the assignments of the irreducible representations to the given states or correctness of the numerical procedures used to obtain the CFP sets from fittings. Some inconsistencies in the previously established sequences of energy levels of Tm^{3+} in both KGdW [9] and KLuW [45] have been mentioned by Pujol *et al* [22]. The differences in the observed energy levels, quoting [22]: '*correspond to either the removal of uncertain and low intense energy levels or to the revision of formerly indicated light polarizations under which they were observed*'.

In view of Burdick's *et al* intensity studies, see, e.g., [46, 47], indicating a plethora of multiple local minima that fit the data nearly equally well, it is rather surprising that only single-fitting results were reported in most cases (for references, see, e.g., [15, 33, 34]). It may be possible that any controversial CFP sets may represent two different closely lying local minima. Repeating the fittings using the original experimental energy levels may result in CFP sets being closer

Table 2. The original ($S1$) theoretical (SOM) and experimental (fit) CFP sets (cm^{-1}) in the Wybourne notation for Tm^{3+} in $KGd(WO_4)_2$ [22] together with the alternative CFP sets ($S2$–$S6$), rhombicity ratios κ and rotational invariants S_k (cm^{-1}). Standard sets are indicated by an asterisk '*'; the dash (—) denotes non-applicable data items. Values in parentheses are the estimated standard deviations for the original fitted set $S1$.

Set #	SOM: $S1/S3$	$S2^*/S5$	$S4/S6$	Fit: $S1/S3$	$S2^*/S5$	$S4/S6$
B_{20}	447	−561.5	114.5	299(16)	−594.1	295.1
Re B_{22}	±276	∓135.7	∓411.7	±363(11)	∓1.6	∓364.6
κ	±0.617	±0.242	∓3.596	±1.214	±0.003	∓1.236
B_{40}	−783	−258.8	−684.1	−893(26)	−344.1	−401.0
Re B_{41}/ Im B_{41}	—	±29.2	±491.3	—	∓19.2	∓497.2
Re B_{42}	±269	∓62.6	∓331.6	±36(26)	∓311.2	∓347.2
Im B_{42}	−736	—	—	−676(19)	—	—
Re B_{43}/ Im B_{43}	—	775.8	601.1	—	729.9	534.8
Re B_{44}	−170	−608.6	−252.8	−36(28)	−495.3	−447.7
Im B_{44}	±247	—	—	±276(29)	—	—
B_{60}	−211	38.8	−17.8	−27(39)	−9.7	221.6
Re B_{61}/ Im B_{61}	—	±168.9	±148.2	—	±215.8	±112.7
Re B_{62}	±205	∓171.7	±279.8	±231(32)	∓113.9	±178.8
Im B_{62}	108	—	—	48(30)	—	—
Re B_{63}/ Im B_{63}	—	4.9	−28.0	—	26.9	−136.1
Re B_{64}	79	145.8	130.6	−139(28)	−134.4	−72.6
Im B_{64}	±24	—	—	±119(28)	—	—
Re B_{65}/ Im B_{65}	—	±89.5	±117.7	—	∓12.2	±127.4
Re B_{66}	∓168	±217.4	∓57.1	∓34(37)	±207.7	∓111.4
Im B_{66}	156	—	—	176(28)	—	—
S_k	$S_2 = 265$	$S_4 = 474$	$S_6 = 144$	$S_2 = 266$	$S_4 = 456$	$S_6 = 137$

to each other. However, it should be kept in mind that even for a very well-studied system, namely $LiYF_4$ doped with a number of RE^{3+} ions, the CFPs even for the same ion reported by various authors reveal large disparities [48].

4. Comparative analysis of CFPs for Tm^{3+} ions in KGdW and KLuW, and Ho^{3+} and Er^{3+} ions in KGdW

For each original theoretical and experimental CFP set for Tm^{3+} ions in KGdW and KLuW [22] five correlated alternative CFP sets have been additionally determined as listed in tables 2 and 3, respectively. Similarly the alternative CFP sets for the CFP sets fitted for Ho^{3+} and Er^{3+} ions in KGdW [23] are listed in table 4. The monoclinic standardization transformations $S2-S6$ [14, 16] are performed using the CST package [32]. At first glance the existence of such alternative CFP sets (tables 2 and 3) appears to hinder achieving unique fittings. However, it is a blessing in disguise and may be used as an advantage. These sets may be utilized within the multiple correlated fitting technique (MCFT) originally proposed in [16] and extended in [18]. The cornerstone of the MCFT is the procedure [16, 18] based on several independent fittings in distinct regions of the CFP space, which enables us to improve the reliability of the final fitted results. The MCFT has been applied successfully for several RE^{3+} ion–host systems [15, 17, 20]. The fittings may be performed using any of the sets $S1$–$S6$ in tables 2–4 as the starting set and varying all CFPs. The recent study [20] indicates that such fittings converge into nearly the same solution (within the parameter uncertainty) after transformation into the standard range. Each fitted solution yielded almost identical values of the invariants S_k [16, 18] and the same r.m.s. deviation of 11.1 cm^{-1} [20]. This indicates convincingly that the minimum that is closest to the starting point is well defined, with the starting point being near neither an inflection point nor a saddle point between multiple local minima.

This appears to not be the case for the fitted CFP sets for Tm^{3+} ions in KGdW and KLuW determined by Pujol *et al* [22]. The disparity between the model CFP sets and the fitted ones in [22] is quantified by the rhombicity ratio listed in tables 2 and 3. The model CFPs and the fitted CFPs for RE^{3+} ions in both crystals [22, 23] turn out to be non-standard [14, 16]. Importantly, the model and fitted CFP sets for Tm-KLuW belong to disparate regions of the CFP space and thus are *intrinsically incompatible* [21]. Thus the two types of CFP sets [22] should not be directly compared [17, 18, 21] and hence, as discussed below, explanation of this disparity must be sought elsewhere.

Since the CFP sets [22, 23] concern RE ions in the same and structurally close crystals, it is worthwhile to quantitatively compare the standardized CFP sets using the closeness factors and the norms ratios defined in [18, 15]; see modifications in [33]. These quantities are calculated in table 5 for each pair of the standardized CFPs in tables 2–4. The norm ratios are selected so that the values would be confined in the range 0–1 in [18, 15, 33]. Generally, all standardized sets appear to be close for $k = 2$ and 4: however, larger differences are observed for $k = 6$. Importantly, the same 'comparability' in terms of the closeness factors and the norms ratios that is obtained for the sets expressed in the standard region should

Table 3. The original ($S1$) theoretical (SOM) and experimental (fit) CFP sets (cm^{-1}) in the Wybourne notation for Tm^{3+} in $KLu(WO_4)_2$ together with the alternative CFP sets ($S2$–$S6$) and rotational invariants S_k. For other explanations see table 2.

Set #	SOM: $S1/S3$	$S2^*/S5$	$S4/S6$	Fit: $S1/S3$	$S2/S5^*$	$S4/S6$
B_{20}	441	−695.7	254.7	332(17)	−670.6	338.6
Re B_{22}	±388	∓76.1	∓464.1	±412(11)	±2.692	∓409.31
κ	±0.880	±0.109	∓1.822	1.241	∓0.004	∓408.908
B_{40}	−905	−429.5	−1058.8	−976(31)	−344.08	−467.41
Re B_{41}/ Im B_{41}	—	±114.8	±388.0	—	∓67.03	±595.24
Re B_{42}	±398	±97.2	∓300.8	±78(28)	∓321.66	∓399.66
Im B_{42}	−711	—	—	−747(19)	—	—
Re B_{43}/ Im B_{43}	—	716.7	613.5	—	823.91	573.60
Re B_{44}	−387	−784.9	−258.4	−38(27)	−566.70	−463.52
Im B_{44}	±146	—	—	±354(33)	—	—
B_{60}	−97	88.1	248.9	−31(41)	126.39	−42.472
Re B_{61}/ Im B_{61}	—	±200.7	±149.6	—	±151.91	±98.213
Re B_{62}	±170	∓46.4	±176.0	±104(32)	∓148.0	±183.60
Im B_{62}	63	—	—	−8(30)	—	—
Re B_{63}/ Im B_{63}	—	−9.9	−90.7	—	−28.797	−113.69
Re B_{64}	−197	−147.5	−104.6	−46(36)	−3.9355	−49.066
Im B_{64}	±59	—	—	±62(29)	—	—
Re B_{65}/ Im B_{65}	0	±36.0	±105.2	0	∓27.185	±45.517
Re B_{66}	∓30	±213.3	∓21.2	∓159(33)	±93.741	∓40.937
Im B_{66}	185	—	—	144(33)	—	—
S_k	$S_2 = 315$	$S_4 = 526$	$S_6 = 133$	$S_2 = 300$	$S_4 = 509$	$S_6 = 99$

Table 4. The original ($S1$) experimental (fit) CFP sets (cm^{-1}) in the Wybourne notation for Ho^{3+} and Er^{3+} ions in $KGd(WO_4)_2$ [23] together with the alternative CFP sets ($S2$–$S6$), rhombicity ratios κ and rotational invariants S_k. For other explanations see table 2.

Ion	Ho^{3+}			Er^{3+}		
Set #	$S1/S3$	$S2/S5^*$	$S4/S6$	$S1/S3$	$S2^*/S5$	$S4/S6$
B_{20}	286(24)	−580.2	294.2	303(28)	−469.93	166.93
Re B_{22}	±357(17)	±3.4	∓353.6	±260	∓55.55	∓315.6
κ	±1.248	∓0.006	∓1.202	±0.858	±0.118	∓1.891
B_{40}	−724(29)	−37.2	−244.3	−986(47)	−88.53	−128.1
Re B_{41}/ Im B_{41}	—	∓66.8	±578.7	—	∓69.66	±643.1
Re B_{42}	±131(34)	∓303.4	∓434.4	±25(63)	∓542.6	∓567.61
Im B_{42}	−724(19)	—	—	−811(30)	—	—
Re B_{43}/ Im B_{43}	—	799.2	555.3	—	893.3	623.9
Re B_{44}	125(29)	−449.6	−276.3	250(53)	−500.9	−467.8
Im B_{44}	±345(24)	—	—	±381(38)	—	—
B_{60}	−60(33)	63.2	−135.2	36(67)	38.8	−68.3
Re B_{61}/ Im B_{61}	—	±24.7	±113.9	—	±58.6	±70.7
Re B_{62}	±256(28)	∓322.7	±334.5	±173(51)	∓224.6	±199.8
Im B_{62}	−241(24)	—	—	−229(38)	—	—
Re B_{63}/ Im B_{63}	—	−267.7	−126.7	—	−196.3	−177.2
Re B_{64}	78(31)	110.9	57.9	5(63)	5.74	−22.875
Im B_{64}	∓103(38)	—	—	∓14(62)	—	—
Re B_{65}/ Im B_{65}	—	∓118.7	∓239.5	—	∓162.1	∓178.5
Re B_{66}	∓277(26)	±178.0	∓160.6	∓173(42)	±96.51	∓133.2
Im B_{66}	133(31)	—	—	125(44)	—	—
S_k	$S_2 = 260$	$S_4 = 457$	$S_6 = 191$	$S_2 = 213$	$S_4 = 548$	$S_6 = 141$

also be obtained for the respective CFP sets in each of the five non-standard regions. However, calculations of these quantities for any pair of the CFPs belonging to disparate regions of the CFP space would be meaningless. Analysis of data in table 5 may be linked with an inspection of the original experimental CFP sets in [22, 23], which reveals what follows. Significant uncertainties may be noticed in the values of several CFPs, in some cases comparable or even

Table 5. The closeness factors and the norm ratios—global (gl) and for rank $k = 2, 4$, and 6—for each pair of the standardized (*) CFP sets in tables 2–4 denoted: (1) SOM Tm:KGdW, (2) fit Tm:KGdW, (3) SOM Tm:KluW, (4) fit Tm:KLuW, (5) fit Ho:KGdW, and (6) fit Er:KGdW.

	Closeness factors						Norm ratios				
	(1, 2)	(1, 3)	(1, 4)	(1, 5)	(1, 6)		(1, 2)	(1, 3)	(1, 4)	(1, 5)	(1, 6)
gl	0.9569	0.9735	0.9491	0.9084	0.8757	gl	0.9325	0.8224	0.9083	0.9844	0.8291
2	0.9475	0.9846	0.9481	0.9489	0.9866	2	0.9976	0.7105	0.7830	0.9561	0.6447
4	0.9594	0.9797	0.9675	0.9443	0.8943	4	0.9247	0.8119	0.8658	0.9283	0.7474
6	0.9521	0.9198	0.8323	0.7134	0.6553	6	0.8991	0.8495	0.4681	0.5722	0.9517
	(2, 3)	(2, 4)	(2, 5)	(2, 6)	(5, 6)		(2, 3)	(2, 4)	(2, 5)	(2, 6)	(5, 6)
gl	0.9512	0.9805	0.9198	0.9214	0.9645	gl	0.7669	0.8470	0.9179	0.7731	0.8423
2	0.9888	1.0000	1.0000	0.9869	0.9876	2	0.7122	0.7848	0.9538	0.6432	0.6743
4	0.9442	0.9984	0.9699	0.9657	0.9857	4	0.7508	0.8007	0.9962	0.6912	0.6938
6	0.9627	0.8129	0.6067	0.5312	0.9441	6	0.9449	0.5206	0.5145	0.9447	0.5446
	(3, 4)	(3, 5)	(3, 6)	(4, 5)	(4, 6)		(3, 4)	(3, 5)	(3, 6)	(4, 5)	(4, 6)
gl	0.9457	0.8555	0.8333	0.9298	0.9425	gl	0.9054	0.8355	0.9920	0.9228	0.9128
2	0.9891	0.9895	0.9999	1.0000	0.9872	2	0.9074	0.6793	0.4581	0.7486	0.5048
4	0.9526	0.8985	0.8581	0.9765	0.9666	4	0.9377	0.7537	0.9205	0.8037	0.8632
6	0.7589	0.5092	0.4364	0.6828	0.7055	6	0.5510	0.4861	0.8926	0.2678	0.4918

exceeding the values of fitted CFPs (see tables 2–4). The values of the quantities C_k and R_k ($k = 2, 4, 6$) and the global factors C_{gl} and R_{gl} in table 5 for the pairs of standardized CFP sets reflect the relatively poor closeness of some of the theoretical and experimental CFP sets. It may be expected that using the CFP sets, which could be obtained using the SOM calculations based on the C approach as proposed in section 3, as initial sets for independent fittings in five other *Si* regions of the CFP space using MCFT would indicate a better overall compatibility of the final fitted CFP sets with the respective initial ones.

The intrinsic properties of the orthorhombic and monoclinic CFPs [14, 15] underlie the problems evident in [22, 23], which concern interpretation of CFP values in terms of structural data. In view of the standardized CFP sets, all statements based on the non-standard values of B_{20} and Re B_{22}, which may potentially belong to disparate regions in the CFP space, must be reconsidered using intrinsically compatible sets. This may be achieved most conveniently using the standardized sets. Let us consider specific examples of such statements identified in [22]. Statement (i): '*Differences between the sets of CF parameters for* Tm^{3+} *in KGdW and KLuW crystals reflect specific crystallographic features of the* C_2 *sites they are occupying. Larger values of* B_0^2 (i.e. B_{20}) *and* B_2^2 (i.e. Re B_{22}) *parameters for KLuW suggest a more ionic and distorted* Tm^{3+} *short-range environment than in KGdW*.' An inspection of the standardized CFP sets in tables 2 and 3 reveals that this statement remains only partially valid. Larger values of B_{20} are obtained for KLuW for both the SOM-derived and fitted CFP sets: however, the SOM parameter Re B_{22} for KLuW is significantly smaller than that for KGdW. Interestingly, for each system the standardized fitted CFP Re B_{22} is close to zero and in comparison with the values of B_{20} it is virtually negligible. This indicates an effective tetragonal-like symmetry of the fitted second-rank CFP sets.

Statement (ii): '*As shown in figure 4(a), an evolution to nearly constant magnitude can describe the behaviour of short-range* B_{20} *parameters from* $4f^2$ *to* $4f^{12}$ *configurations, while somewhat higher magnitudes can describe the same behaviour in* B_{22} *parameters. It seems that the CF weakening due to the nuclear charge increase criterion is compensated, and for* B_{22} *even surpassed, by its enhancement derived of the reduction of some RE–O distance from* Pr^{3+} *to* Tm^{3+}*-doped crystals*'. Consideration of the problems concerning the variation of the 'phenomenological' CFPs for RE ions in RE-KGdW crystals across the $4f^N$ series, presented in figure 4(a) of [22] and figure 1 of [23], requires reanalysis of the CFP sets for Pr^{3+} and Nd^{3+} ions in other $AB(WO_4)_2$ crystals [24–26], in addition to the CFP sets for Tm^{3+} ions in KGdW and KLuW, and Ho^{3+} and Er^{3+} ions in KGdW dealt with here. This reanalysis will be carried out in Part II. Here we note only that the authors [22, 23] did not ascertain the *intrinsic* comparability of the CFP sets used in the systematics across the RE series. Such indiscriminate usage of CFP sets taken from various sources may be misleading.

5. Summary and conclusions

The crystal-field (CF) analysis of optical absorption spectra carried out by Pujol *et al* for Tm^{3+} ions in $KGd(WO_4)_2$ (KGdW) and $KLu(WO_4)_2$ (KLuW) single crystals [22], and Ho^{3+} and Er^{3+} ions in KGdW [23] have been revisited in this Part I. Simultaneous fittings of the 24 parameters, with some constraints on the free-ion parameters, and CF Hamiltonian for the actual C_2 symmetry of the metal site have been carried out [22, 23] using the reduced (R)

approach [16, 18], i.e. with the second-rank CF parameter Im B_{22} set to zero. The initial CFPs for fittings were calculated in [22] using the simple overlap model (SOM) assuming inappropriately the R approach, instead of the complete (C) approach [16, 18].

To overcome the difficulties encountered in the CF studies [22, 23], we propose a consistent methodology for CF analysis for transition ions at monoclinic symmetry (C_s, C_2, C_{2h}) sites in crystals, which takes into account the intrinsic properties of the orthorhombic [14, 15] and monoclinic CF Hamiltonians [16–20]. These properties bear significantly on the meaningfulness of CF studies and interpretation of the resulting CFPs. An apparent lack of awareness of these properties by some authors, including Pujol *et al* [22, 23], may lead to misinterpretation of the model and fitted CFPs determined for various RE^{3+} ions in $KRE(WO_4)_2$ crystals. Consistent and accurate modelling of CF interactions is indispensable to establish the correct $4f^{12}$ Tm^{3+} configuration in a given crystal host. Disregarding the intrinsic CFP properties in CF analysis for orthorhombic and lower symmetry can lead to errors in the evaluation of the spectroscopic parameters involved in laser operation [22].

Critical examination of the study [22] has also revealed several other doubtful aspects, some of which apply also for the study [23]. These aspects, clarified in this Part, concern (i) notation for CFP symbols, (ii) distinction between the meaning of the symbolic, model and fitted CFPs, (iii) relative orientation of the axis system used in the SOM calculations w.r.t. the crystallographic axes, (iv) appropriateness of the specific monoclinic CF Hamiltonian form employed, (v) interpretation and appropriateness of the R approach versus the C approach and (vi) general reasons for disparities between CFP sets.

Comparative analysis of CFPs reveals the importance of proper definitions of the axis system used in model calculations of CFPs and the *nominal* meaning of the axis systems assigned to the fitted CFPs. The present methodology may be considered as a general framework for analysis of CF levels and modelling of CFPs for rare-earth ions at monoclinic symmetry sites. CFP sets for Pr^{3+} and Nd^{3+} ions in other $AB(WO_4)_2$ crystals [24–26] will be dealt with in Part II, whereas other relevant CFP sets for RE^{3+} ions at monoclinic symmetry sites reported in the literature may also need critical examination as reviewed in [21].

Acknowledgments

This work was partially supported by the research grant from the Polish Ministry of Science and Tertiary Education in the years 2006–2009. Thanks are due to Mrs H Dopierała for technical help with tables and references.

Appendix A. Choices for assigning orthorhombic symmetry axes

Figure A.1 presents a diagram depicting the six choices for assigning orthorhombic axes ($\pm a_1, \pm a_2, \pm a_3$) to a Cartesian axis system: $S1(x, y, z)$, $S2(x, -z, y)$, $S3(y, x, -z)$, $S4(y, z, x)$, $S5(z, x, y)$, $S6(-z, y, x)$, while adhering to the right-handed axis system convention. Ranges of the original rhombicity ratio $\{\lambda' = B_2^2/B_2^0\}$ in the extended Stevens operator notation and $\{\kappa = \mathrm{Re}\, B_{22}/B_{20}\}$ in the Wybourne notation, and the transformation angles corresponding to each choice, are also indicated in figure A.1; for references and explanations, see section 2.

Appendix B. Orthorhombic and monoclinic standardization transformations of CFPs in the Wybourne notation

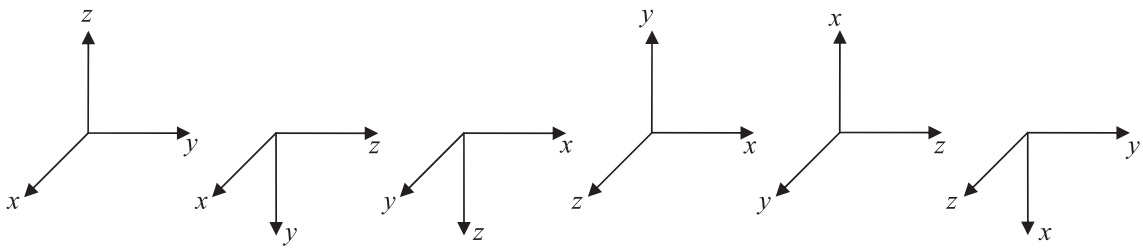

Designation of the transformed axis system:

Si:	S1	S2	S3	S4	S5	S6

Ranges of the original $\{\lambda'\}$ for which the corresponding transformation Si defined above yields the ratio $[\lambda']$ and $[\kappa]$ for the transformed CFP set in the standard range (0, 1) and (0, p ≡ $1/\sqrt{6}$):

$\{\lambda'\}$:	(0, 1)	(1, 3)	(-1, 0)	(-3, -1)	(3, ∞)	(-∞, -3)
$\{\kappa\}$:	(0, p)	(p, 3p)	(-p, 0)	(-3p, -p)	(3p, ∞)	(-∞, -3p)

The azimuthal (φ_i) and polar (θ_i) angles corresponding to a given Si transformation defined above:

(φ_1, θ_1):	(-π/2, -π/2)	(-π/2, π)	(0, π/2)	(-π/2, -π/2)	(0, π/2)
(φ_2, θ_2):	(π/2, 0)	(0, 0)	(π/2, 0)	(0, 0)	(0, 0)

Figure A.1. Definition of the axis systems used for standardization and their interrelationships.

Table B.1. Standardization transformations Si for the original orthorhombic CFPs $\{B_{kq}\}$ expressed in the Wybourne notation based on limiting the rhombicity ratio $[\kappa] = [\mathrm{Re}\, B_{22}]/[B_{20}]$ for the transformed CFPs $[B_{kq}]$ within the standard range $(0, 1/\sqrt{6})$. The long dash (—) denotes non-applicable data items.

	Transformed system	$S6$ (upper sign)/$S4$ (lower sign)	$S3$	$S2$ (upper sign)/$S5$ (lower sign)
B_{20}	$[B_{20}]$	$-\frac{1}{2}\{B_{20}\} + \frac{\sqrt{6}}{2}\{\mathrm{Re}\, B_{22}\}$	$\{B_{20}\}$	$-\frac{1}{2}\{B_{20}\} - \frac{\sqrt{6}}{2}\{\mathrm{Re}\, B_{22}\}$
Re B_{21}	—	—/$\{\mathrm{Im}\, B_{22}\}$	—	$\{\mathrm{Im}\, B_{22}\}$/—
Im B_{21}	—	$-\{\mathrm{Im}\, B_{22}\}$/—	—	—/$-\{\mathrm{Im}\, B_{22}\}$
Re B_{22}	$[\mathrm{Re}\, B_{22}]$	$\pm(\frac{\sqrt{6}}{4}\{B_{20}\} + \frac{1}{2}\{\mathrm{Re}\, B_{22}\})$	$\{-\mathrm{Re}\, B_{22}\}$	$\pm(-\frac{\sqrt{6}}{4}\{B_{20}\} + \frac{1}{2}\{\mathrm{Re}\, B_{22}\})$
Im B_{22}	$[\mathrm{Im}\, B_{22}]$	—	$\{\mathrm{Im}\, B_{22}\}$	—
B_{40}	$[B_{40}]$	$\frac{3}{8}\{B_{40}\} - \frac{\sqrt{10}}{4}\{\mathrm{Re}\, B_{42}\} + \frac{\sqrt{70}}{8}\{\mathrm{Re}\, B_{44}\}$	$\{B_{40}\}$	$\frac{3}{8}\{B_{40}\} + \frac{\sqrt{10}}{4}\{\mathrm{Re}\, B_{42}\} + \frac{\sqrt{70}}{8}\{\mathrm{Re}\, B_{44}\}$
Re B_{41}	—	—/$-\frac{\sqrt{2}}{4}\{\mathrm{Im}\, B_{42}\} + \frac{\sqrt{14}}{4}\{\mathrm{Im}\, B_{44}\}$	—	$-\frac{\sqrt{2}}{4}\{\mathrm{Im}\, B_{42}\} - \frac{\sqrt{14}}{4}\{\mathrm{Im}\, B_{44}\}$/—
Im B_{41}	—	$\frac{\sqrt{2}}{4}\{\mathrm{Im}\, B_{42}\} - \frac{\sqrt{14}}{4}\{\mathrm{Im}\, B_{44}\}$/—	—	—/$\frac{\sqrt{2}}{4}\{\mathrm{Im}\, B_{42}\} + \frac{\sqrt{14}}{4}\{\mathrm{Im}\, B_{44}\}$
Re B_{42}	$[\mathrm{Re}\, B_{42}]$	$\pm(-\frac{\sqrt{10}}{8}\{B_{40}\} + \frac{1}{2}\{\mathrm{Re}\, B_{42}\} + \frac{\sqrt{7}}{4}\{\mathrm{Re}\, B_{44}\})$	$\{-\mathrm{Re}\, B_{42}\}$	$\pm(\frac{\sqrt{10}}{8}\{B_{40}\} + \frac{1}{2}\{\mathrm{Re}\, B_{42}\} - \frac{\sqrt{7}}{4}\{\mathrm{Re}\, B_{44}\})$
Im B_{42}	$[\mathrm{Im}\, B_{42}]$	—	$\{\mathrm{Im}\, B_{42}\}$	—
Re B_{43}	—	—/$-\frac{\sqrt{14}}{4}\{\mathrm{Im}\, B_{42}\} - \frac{\sqrt{2}}{4}\{\mathrm{Im}\, B_{44}\}$	—	$-\frac{\sqrt{14}}{4}\{\mathrm{Im}\, B_{42}\} + \frac{\sqrt{2}}{4}\{\mathrm{Im}\, B_{44}\}$/—
Im B_{43}	—	$-\frac{\sqrt{14}}{4}\{\mathrm{Im}\, B_{42}\} - \frac{\sqrt{2}}{4}\{\mathrm{Im}\, B_{44}\}$/—	—	—/$-\frac{\sqrt{14}}{4}\{\mathrm{Im}\, B_{42}\} + \frac{\sqrt{2}}{4}\{\mathrm{Im}\, B_{44}\}$
Re B_{44}	$[\mathrm{Re}\, B_{44}]$	$\frac{\sqrt{70}}{16}\{B_{40}\} + \frac{\sqrt{7}}{4}\{\mathrm{Re}\, B_{42}\} + \frac{1}{8}\{\mathrm{Re}\, B_{44}\}$	$\{\mathrm{Re}\, B_{44}\}$	$\frac{\sqrt{70}}{16}\{B_{40}\} - \frac{\sqrt{7}}{4}\{\mathrm{Re}\, B_{42}\} + \frac{1}{8}\{\mathrm{Re}\, B_{44}\}$
Im B_{44}	$[\mathrm{Im}\, B_{44}]$	—	$\{-\mathrm{Im}\, B_{44}\}$	—
B_{60}	$[B_{60}]$	$-\frac{5}{16}\{B_{60}\} + \frac{\sqrt{105}}{16}\{\mathrm{Re}\, B_{62}\} - \frac{3\sqrt{14}}{16}\{\mathrm{Re}\, B_{64}\} + \frac{\sqrt{231}}{16}\{\mathrm{Re}\, B_{66}\}$	$\{B_{60}\}$	$-\frac{5}{16}\{B_{60}\} - \frac{\sqrt{105}}{16}\{\mathrm{Re}\, B_{62}\} - \frac{3\sqrt{14}}{16}\{\mathrm{Re}\, B_{64}\} - \frac{\sqrt{231}}{16}\{\mathrm{Re}\, B_{66}\}$
Re B_{61}	—	—/$\frac{\sqrt{10}}{16}\{\mathrm{Im}\, B_{62}\} - \frac{\sqrt{3}}{4}\{\mathrm{Im}\, B_{64}\} + \frac{3\sqrt{22}}{16}\{\mathrm{Im}\, B_{66}\}$	—	$\frac{\sqrt{10}}{16}\{\mathrm{Im}\, B_{62}\} + \frac{\sqrt{3}}{4}\{\mathrm{Im}\, B_{64}\} + \frac{3\sqrt{22}}{16}\{\mathrm{Im}\, B_{66}\}$/—
Im B_{61}	—	$\frac{\sqrt{10}}{16}\{\mathrm{Im}\, B_{62}\} - \frac{\sqrt{3}}{4}\{\mathrm{Im}\, B_{64}\} + \frac{3\sqrt{22}}{16}\{\mathrm{Im}\, B_{66}\}$/—	—	—/$\frac{\sqrt{10}}{16}\{\mathrm{Im}\, B_{62}\} + \frac{\sqrt{3}}{4}\{\mathrm{Im}\, B_{64}\} + \frac{3\sqrt{22}}{16}\{\mathrm{Im}\, B_{66}\}$
Re B_{62}	$[\mathrm{Re}\, B_{62}]$	$\pm(\frac{\sqrt{105}}{32}\{B_{60}\} - \frac{17}{32}\{\mathrm{Re}\, B_{62}\} + \frac{\sqrt{30}}{32}\{\mathrm{Re}\, B_{64}\} + \frac{3\sqrt{55}}{32}\{\mathrm{Re}\, B_{66}\})$	$\{-\mathrm{Re}\, B_{62}\}$	$\pm(-\frac{\sqrt{105}}{32}\{B_{60}\} - \frac{17}{32}\{\mathrm{Re}\, B_{62}\} - \frac{\sqrt{30}}{32}\{\mathrm{Re}\, B_{64}\} + \frac{3\sqrt{55}}{32}\{\mathrm{Re}\, B_{66}\})$
Im B_{62}	$[\mathrm{Im}\, B_{62}]$	—	$\{\mathrm{Im}\, B_{62}\}$	—
Re B_{63}	—	—/$\frac{9}{16}\{\mathrm{Im}\, B_{62}\} - \frac{\sqrt{30}}{8}\{\mathrm{Im}\, B_{64}\} - \frac{\sqrt{55}}{16}\{\mathrm{Im}\, B_{66}\}$	—	$\frac{9}{16}\{\mathrm{Im}\, B_{62}\} + \frac{\sqrt{30}}{8}\{\mathrm{Im}\, B_{64}\} - \frac{\sqrt{55}}{16}\{\mathrm{Im}\, B_{66}\}$/—
Im B_{63}	—	$-\frac{9}{16}\{\mathrm{Im}\, B_{62}\} + \frac{\sqrt{30}}{8}\{\mathrm{Im}\, B_{64}\} + \frac{\sqrt{55}}{16}\{\mathrm{Im}\, B_{66}\}$/—	—	—/$-\frac{9}{16}\{\mathrm{Im}\, B_{62}\} - \frac{\sqrt{30}}{8}\{\mathrm{Im}\, B_{64}\} + \frac{\sqrt{55}}{16}\{\mathrm{Im}\, B_{66}\}$
Re B_{64}	$[\mathrm{Re}\, B_{64}]$	$-\frac{3\sqrt{14}}{32}\{B_{60}\} + \frac{\sqrt{30}}{32}\{\mathrm{Re}\, B_{62}\} + \frac{13}{16}\{\mathrm{Re}\, B_{64}\} + \frac{\sqrt{66}}{32}\{\mathrm{Re}\, B_{66}\}$	$\{\mathrm{Re}\, B_{64}\}$	$-\frac{3\sqrt{14}}{32}\{B_{60}\} - \frac{\sqrt{30}}{32}\{\mathrm{Re}\, B_{62}\} + \frac{13}{16}\{\mathrm{Re}\, B_{64}\} - \frac{\sqrt{66}}{32}\{\mathrm{Re}\, B_{66}\}$
Im B_{64}	$[\mathrm{Im}\, B_{64}]$	—	$\{-\mathrm{Im}\, B_{64}\}$	—
Re B_{65}	—	—/$\frac{\sqrt{165}}{16}\{\mathrm{Im}\, B_{62}\} + \frac{\sqrt{22}}{8}\{\mathrm{Im}\, B_{64}\} + \frac{\sqrt{3}}{16}\{\mathrm{Im}\, B_{66}\}$	—	$\frac{\sqrt{165}}{16}\{\mathrm{Im}\, B_{62}\} - \frac{\sqrt{22}}{8}\{\mathrm{Im}\, B_{64}\} + \frac{\sqrt{3}}{16}\{\mathrm{Im}\, B_{66}\}$/—
Im B_{65}	—	$\frac{\sqrt{165}}{16}\{\mathrm{Im}\, B_{62}\} + \frac{\sqrt{22}}{8}\{\mathrm{Im}\, B_{64}\} + \frac{\sqrt{3}}{16}\{\mathrm{Im}\, B_{66}\}$/—	—	—/$\frac{\sqrt{165}}{16}\{\mathrm{Im}\, B_{62}\} - \frac{\sqrt{22}}{8}\{\mathrm{Im}\, B_{64}\} + \frac{\sqrt{3}}{16}\{\mathrm{Im}\, B_{66}\}$
Re B_{66}	$[\mathrm{Re}\, B_{66}]$	$\pm(\frac{\sqrt{231}}{32}\{B_{60}\} + \frac{3\sqrt{55}}{32}\{\mathrm{Re}\, B_{62}\} + \frac{\sqrt{66}}{32}\{\mathrm{Re}\, B_{64}\} + \frac{1}{32}\{\mathrm{Re}\, B_{66}\})$	$\{-\mathrm{Re}\, B_{66}\}$	$\pm(-\frac{\sqrt{231}}{32}\{B_{60}\} + \frac{3\sqrt{55}}{32}\{\mathrm{Re}\, B_{62}\} - \frac{\sqrt{66}}{32}\{\mathrm{Re}\, B_{64}\} + \frac{1}{32}\{\mathrm{Re}\, B_{66}\})$
Im B_{66}	$[\mathrm{Im}\, B_{66}]$	—	$\{\mathrm{Im}\, B_{66}\}$	—

References

[1] Wybourne B G 1965 *Spectroscopic Properties of Rare Earths* (New York: Interscience)
[2] Hüfner S 1978 *Optical spectra of Transparent Rare Earth Compounds* (New York: Academic)
[3] Powell R C 1998 *Physics of Solid-State Laser Materials* (New York: Springer)
[4] Mulak J and Gajek Z 2000 *The Effective Crystal Field Potential* (Amsterdam: Elsevier)
[5] Newman D J and Ng B 2000 *Crystal Field Handbook* (Cambridge: Cambridge University Press)
[6] Henderson B and Bartram R H 2000 *Crystal-Field Engineering of Solid-State Laser Materials* (Cambridge: Cambridge University Press)
[7] Wildner M, Andrut M and Rudowicz C 2004 Optical absorption spectroscopy in geosciences. Part I: basic concepts of crystal field theory *Spectroscopic Methods in Mineralogy—EMU Notes Mineralogy* vol 6, ed A Beran and E Libowitzky (Budapest: Eötvös University Press) chapter 3, pp 93–143
[8] Görller-Walrand C and Binnemans K 1996 Rationalization of crystal field parametrization *Handbook of the Physics and Chemistry of Rare Earths* vol 23, ed K A Gschneidner Jr and L Eyring (Amsterdam: Elsevier)
[9] Güell F, Mateos X, Gavalda J, Sole R, Aguilo M, Dıaz F and Massons J 2004 *J. Lumin.* **106** 109
[10] Güell F, Mateos X, Gavalda J, Sole R, Aguilo M, Dıaz F, Galan M and Massons J 2004 *Opt. Mater.* **25** 71
[11] Pujol M C, Rico M, Zaldo C, Sole R, Nikolov V, Solans X, Aguilo M and Dıaz F 1999 *Appl. Phys.* B **68** 187
[12] Macalik L, Hanuza J, Jaque D and Garcıa Sole J 2006 *Opt. Mater.* **28** 980
[13] Macalik L, Hanuza J, Macalik B, Ryba-Romanowski W, Golab S and Pietraszko A 1998 *J. Lumin.* **79** 9
[14] Rudowicz C and Bramley R 1985 *J. Chem. Phys.* **83** 5192
[15] Rudowicz C, Gnutek P and Karbowiak M 2007 *Phys. Rev.* B **76** 125116
[16] Rudowicz C 1986 *J. Chem. Phys.* **84** 5045
[17] Rudowicz C, Chua M and Reid M F 2000 *Physica* B **291** 327
[18] Rudowicz C and Qin J 2004 *J. Lumin.* **110** 39
[19] Gnutek P and Rudowicz C 2008 *Opt. Mater.* **31** 391
[20] Mech A, Gajek Z, Karbowiak M and Rudowicz C 2008 *J. Phys.: Condens. Matter* **20** 385205
[21] Rudowicz C and Gnutek P 2010 *Physica* B **405** 113
[22] Pujol M C, Cascales C, Aguiló M and Díaz F 2008 *J. Phys.: Condens. Matter* **20** 345219
[23] Pujol M C, Cascales C, Rico M, Massons J, Dıaz F, Porcher P and Zaldo C 2001 *J. Alloys Compounds* **323/324** 321
[24] Mironov V S and Li L E 1998 *J. Alloys Compounds* **279** 83
[25] Zaldo C, Rico M, Cascales C, Pujol M C, Massons J, Aguilo M, Dıaz F and Porcher P 2000 *J. Phys.: Condens. Matter* **12** 8531
[26] Mendez-Blas A, Rico M, Volkov V, Cascales C, Zaldo C, Coya C, Kling A and Alves L C 2004 *J. Phys.: Condens. Matter* **16** 2139
[27] Porcher P, Couto dos Santos M and Malta O 1999 *Phys. Chem. Chem. Phys.* **1** 397
[28] Malta O L 1982 *Chem. Phys. Lett.* **87** 27
Malta O L 1982 *Chem. Phys. Lett.* **88** 353
[29] Rudowicz C 1987 *Magn. Reson. Rev.* **13** 1
Rudowicz C 1988 *Magn. Reson. Rev.* **13** 335 (erratum)
[30] Rudowicz C and Misra S K 2001 *Appl. Spectrosc. Rev.* **36** 11
[31] Mulak J and Mulak M 2005 *J. Phys. A: Math. Gen.* **38** 6081
[32] Rudowicz C 2000 *Crystal Field Handbook* ed D J Newman and B Ng (Cambridge: Cambridge University Press) p 259
[33] Rudowicz C, Gnutek P, Lewandowska M and Orłowski M 2009 *J. Alloys Compounds* **467** 98
[34] Rudowicz C, Gnutek P and Lewandowska M 2009 *J. Alloys Compounds* **467** 106
[35] Rudowicz C 1985 *Chem. Phys.* **97** 43
[36] Rudowicz C 1985 *J. Phys. C: Solid State Phys.* **18** 1415
Rudowicz C 1985 *J. Phys. C: Solid State Phys.* **18** 3837 (erratum)
[37] Newman D J and Ng B 1989 *Rep. Prog. Phys.* **52** 699
[38] Gajek Z and Mulak J 1992 *J. Phys.: Condens. Matter* **4** 427
[39] Gajek Z 2005 *Phys. Rev.* B **67** 045139
[40] Malkin B Z 1987 *Spectroscopy of Solids Containing Rare-Earth* ed A A Kaplyanskii and B M Macfarlane (Amsterdam: North-Holland)
[41] Malta O L 1982 *Chem. Phys. Lett.* **87** 27
Malta O L 1982 *Chem. Phys. Lett.* **88** 353
[42] Porcher P 1989 Fortran Routines REEL and IMAGE for simulation of d^N and f^N *Configurations Involving Real and Complex Crystal-Field Parameters* Paris unpublished
[43] Burdick G W and Reid M F 2004 *Mol. Phys.* **102** 1141
[44] Chang N C, Gruber J B, Leavitt R P and Morrison C A 1982 *J. Chem. Phys.* **76** 3877
[45] Silvestre O, Pujol M C, Rico M, Güell F, Aguilo M and Dıaz F 2007 *Appl. Phys.* B **87** 707
[46] Burdick G W, Crooks S M and Reid M F 1999 *Phys. Rev.* B **59** 7789
[47] Burdick G W, LaBianca E S and Binus D L 2002 *J. Alloys Compounds* **344** 327
[48] Rudowicz C and Qin J 2004 *J. Alloys Compounds* **385** 238